Journal of Power Sources 227 (2013) 300–308

Contents lists available at SciVerse ScienceDirect

Journal of Power Sources

journal homepage: www.elsevier.com/locate/jpowsour

Differentiate the pseudocapacitance and double-layer capacitance contributions for nitrogen-doped reduced graphene oxide in acidic and alkaline electrolytes

Ying-Hui Lee, Kuo-Hsin Chang, Chi-Chang Hu*

Laboratory of Electrochemistry and Advanced Materials, Department of Chemical Engineering, National Tsing Hua University, Hsin-Chu 30013, Taiwan

HIGHLIGHTS

- The effects of N-doped groups are more pronounced in acids than in alkaline media.
- Pseudocapacitance from pyridinic-/pyrrolic-N is observed negative to 0.6 V in acids.
- Nitrogen-doped groups contribute higher C_{dl} in H_2SO_4 compared to that in KOH.
- N-RGO as anodes in both acidic and alkaline media results in high specific energy.

GRAPHICAL ABSTRACT

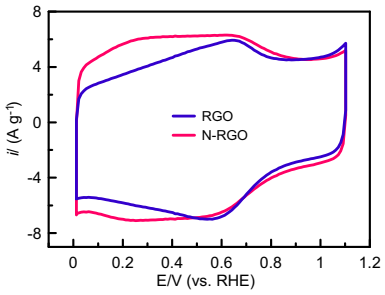

ARTICLE INFO

Article history:
Received 21 June 2012
Received in revised form
27 September 2012
Accepted 12 November 2012
Available online 23 November 2012

Keywords:
N-doped reduced graphene oxide
Nitrogen-containing functional group
Pseudocapacitance
Double-layer capacitance
Aqueous electrolyte

ABSTRACT

Nitrogen-doped reduced graphene oxide (N-RGO) and reduced graphene oxide (RGO) have been synthesized by microwave-assisted hydrothermal method to discern the actual contribution of nitrogen-containing functional groups on the specific capacitance ($C_{S,T}$) in acidic and alkaline electrolytes. Material characterization reveals similar porosity, electrolyte-accessible surface area, element composition, and graphitic crystallinity between N-RGO and RGO except the difference in the nitrogen content. In 1 M H_2SO_4, additional pseudocapacitance provided by pyridinic-N and pyrrolic-N/pyridone-N is clearly observed at the potential negative to 0.6 V (vs. RHE) while this contribution in pseudocapacitance diminishes in 1 M KOH due to the lack of proton in the electrolyte for these basic functional groups to undergo redox reactions. The double-layer capacitance of N-RGO in 1 M H_2SO_4 in higher than that in 1 M KOH owing to the presence of N-containing functional groups which increase the electronic charge density of graphene and favor proton adsorption in the acidic electrolyte. The contribution of nitrogen-containing functional groups on $C_{S,T}$ in acidic media is more pronounced than that in the alkaline electrolyte. This finding is crucial for the future application of N-doped carbons in supercapacitors to achieve full utilization.

1. Introduction

Recently, N-doped carbon materials, such as N-doped porous carbons [1–5], N-doped nonporous carbons [6], N-doped carbon nanotubes [7,8], N-doped graphene [9], etc., have been widely investigated for the application of electric double layer capacitors (EDLCs). Previous study indicated that four forms of nitrogen-containing functional groups appear on the N-doped carbon materials and enhance the capacitive performances, which are pyridinic-N (398.5 eV), pyrrolic-N/pyridone-N (400 eV), quaternary-N (401.2 eV), and pyridine-N-oxide (403 eV) [1,4,10]. Pyridinic-N and pyrrolic-N/pyridone-N are believed to provide pseudocapacitance through the redox reactions involving protons, similar to that of the quinone functional group [6,7,9,11]. Meanwhile, the presence of quaternary-N and pyridine-N-oxide has been

* Corresponding author. Tel./fax: +886 3 5736027.
E-mail address: cchu@che.nthu.edu.tw (C.-C. Hu).
URL: http://mx.nthu.edu.tw/~cchu/

0378-7753/$ – see front matter © 2012 Elsevier B.V. All rights reserved.
http://dx.doi.org/10.1016/j.jpowsour.2012.11.026

proposed to enhance the electron transport through the carbon materials and therefore maintain the superior capacitance retention during the fast charge/discharge process. Both phenomena have been confirmed by the experimental results and the correlations between $C_{S,T}$ and the contents of different nitrogen-containing functional groups were established [1,10]. Therefore, nitrogen-containing functional groups are believed to provide pseudocapacitance (i.e., higher $C_{S,T}$) and enhance the electronic conductivity of the carbon materials in comparison with the non-doped ones.

Unfortunately, few efforts have been made to discern the actual contribution of nitrogen-containing functional groups on the capacitive performances between N-doped and non-doped carbon materials based on the same material characteristics (e.g., porosity, surface area, graphitic crystallinity, etc.). For example, the virtue of nitrogen-containing functional groups in electrolytes with different pH values, the effectiveness in the suitable potential range, and the charge/discharge efficiency in a two-electrode system, etc., still remain unclear. How to effectively utilize the nitrogen-containing functional groups in correct potential regions and desired media for the future application of supercapacitors is an interesting research topic. Thus, the purpose of this work is to synthesize N-doped and non-doped reduced graphene oxides (denoted as N-RGO and RGO, respectively) with similar material characteristics in order to evaluate the actual contribution of nitrogen-containing functional groups from systematic comparisons between these two materials through electrochemical analyses.

In fabricating N-doped and non-doped carbon materials, common preparation methods such as with/without the ammoxidation of certain carbon materials [8,12,13] and the thermal treatment of nitrogen-containing precursor/normal carbon precursors [2,14–16] have been reported. However, the high temperature treatment usually increases the difficulty in controlling the porosity, the oxygen content, and the graphitic crystallinity. Especially, the difference in the oxygen content makes it difficult to discern the contributions of nitrogen-containing functional groups from the oxygen-containing functional groups on the capacitive performance. Accordingly, the microwave-assisted hydrothermal method is employed to synthesize N-RGO and RGO in order to meet the requirement for a fair comparison.

In our previous work [17–19], the microwave-assisted hydrothermal route could directly remove the oxygen-containing functional groups without restoring the defects on the graphene sheets in reducing graphene oxide (GO, the precursor of RGO and N-RGO). Therefore, similarity in the porosity, the oxygen content, and the degree of graphitic crystallinity for RGO and N-RGO is expected to be obtained when the nitrogen-containing molecules (i.e., urea) react with GO to obtain N-RGO through the simultaneous incorporation of nitrogen atoms into graphene sheets during the reduction of GO. The materials characterization, including the nitrogen adsorption/desorption isotherms, transmission electron microscopic (TEM), X-ray photoelectron spectroscopic (XPS), Raman spectroscopic analyses, are used to examine the material similarity between RGO and N-RGO.

2. Experimental

2.1. Preparation of reduced graphene oxide and N-doped reduced graphene oxide

Nanographite platelets (N008-100-N, Angstron Materials Co., USA) with ca. 100 nm in thickness were used as the raw material to prepare graphene oxide (GO). The preparation of GO solutions (ca. 1 mg mL^{-1}) followed the modified Hummers' method with supersonic exfoliation [20,21]. Then, a 10-mL GO solution was well mixed with a 10-mL urea solution (2 mg mL^{-1}) to obtain the precursor solution for preparing N-RGO. The precursor solution was subject to microwave-assisted hydrothermal heating from room temperature to 190 °C and kept at this temperature with an air-flow cooling for 10 min at a constant power of 200 W (i.e., under the PowerMax mode) in a microwave reactor (CEM, USA). Reduced graphene oxide was synthesized via the same microwave-assisted hydrothermal procedure except that the GO solution was mixed with 10 mL deionized water before subject to the microwave-assisted hydrothermal heating.

2.2. Material characterization

The transmission electron microscopic (TEM) images of RGO and N-RGO were obtained by JEM-2010 (JEOL, Japan). The XPS measurements were performed on the PHI Quantera SXM (ULVAC-PHI, Japan) which employed Al monochromator irradiation as the photosource. Raman spectra were recorded on Lab RAM HR (Horoba, France) equipped with a HeNe laser source (wavelength: 633 nm). The N_2 adsorption/desorption isotherms were measured at 77 K using the NOVA 4200*e* (Quantachrome®, USA), which equipped with an automated surface area and pore size analyzer. Before measuring the N_2 adsorption/desorption isotherms, samples were degassed at 200 °C for 12 h.

2.3. Electrochemical measurements

The electrochemical responses of RGO and N-RGO were investigated by CHI 633C (CH Instruments, USA) in both three-electrode and two-electrode modes. Under the three-electrode mode, a Ag/AgCl electrode (Argenthal, 3 M KCl, 0.207 V vs. standard hydrogen electrode at 25 °C) was used as the reference electrode, and a platinum wire was employed as the counter electrode. A Luggin capillary was used to minimize errors due to ohmic potential (*iR*) drop in the electrolyte. The two-electrode systems were designed for measuring the energy and power densities of a single cell of the symmetric form (i.e., N-RGO/N-RGO or RGO/RGO) in the acidic electrolyte and the asymmetric type (N-RGO/Ni–Co hydroxide or RGO/Ni–Co hydroxide) in the alkaline electrolyte.

The material for the working electrode was a mixture consisting of N-RGO (or RGO) and polyvinylidene fluoride (PVDF) in the weight ratio of 10:1. The mixture (ca. 0.5 mg) was homogeneously suspended in N-methyl-2-pyrrolidone and coated on a graphite substrate with an exposed surface area of 1 cm^2. For the single cell of the asymmetric design in the alkaline medium, Ni–Co hydroxides with a similar voltammetric charge to that of a 0.5-mg N-RGO (or RGO) were employed as the positive material, which were prepared by electrochemical deposition. The electrolytes for evaluating the capacitive performances were 1 M H_2SO_4 and 1 M KOH. For convenient comparisons, all electrode potentials reported in this work are related to a reversible hydrogen electrode (RHE).

The specific capacitance ($C_{S,T}$) of RGO and NGRO measured under the three-electrode mode was estimated from the cyclic voltammograms (CVs) based on the following equations:

$$C_S = \frac{Q}{\Delta V \cdot m} = \frac{\int i(\mathrm{d}V/v)}{\Delta V \cdot m} = \frac{\int i\mathrm{d}t}{\Delta V \cdot m} \quad (1)$$

$$C_{S,T} = \frac{C_{S,C} + C_{S,A}}{2} \quad (2)$$

where $C_{S,T}$ is the average specific gravimetric capacitance (F g^{-1}) obtained from positive ($C_{S,A}$) and negative ($C_{S,C}$) sweeps. Q in equation (1) is the voltammetric charge in one sweep, ΔV is the potential

window (i.e., 1.1 V), m is the mass (g) of the sample being coated on the graphite electrode, ν is the scan rate (V s^{-1}). For the two-electrode mode, the specific capacitance was measured from the galvanostatic charge/discharge curves on the basis of equation (3):

$$C_{S,T} = \frac{Q}{\Delta V \cdot m} = \frac{It}{\Delta V \cdot m} \quad (3)$$

where I (A), t (s), and Q represent the discharge current, discharge time, and the charge obtained from the discharge of the two-electrode cell. Here mass is the total mass of both electrodes. Therefore the specific energy density (SE, W h kg^{-1}) and the specific power density (SP, W kg^{-1}) can be obtained from equations (4) and (5):

$$SE = \frac{C_{S,T}(\Delta V)^2}{2} \times \frac{1000}{3600} \quad (4)$$

$$SP = \frac{SE}{t} \times 3600 \quad (5)$$

3. Results and discussion

3.1. Material characterization

To ensure that the only difference between RGO and N-RGO is the nitrogen doping degree, the morphology, the contents of surface functional groups, and the degree of graphitic crystallinity of both graphene materials were carefully examined by utilizing various analytical techniques. From the TEM images shown in Fig. 1A and B, typical sheet-like structures with crumples are found for both RGO and N-RGO. The GO in the precursor solution prepared from the modified Hummers' method demonstrates isolated single-layer GO nanosheets with the thickness of ca. 0.74 nm (see our previous work [22]). However, the microwave-assisted hydrothermal treatment effectively removes the surface oxygen-containing functional groups, leading to the restacking and crumpling of RGO nanosheets. Thus, RGO is of the multi-layered structure instead of an individual single-layered nanosheet. Note that relatively smaller crumpled pieces of nanosheets are observed for N-RGO due to the additional interactions between GO nanosheets and urea molecules under the hydrothermal environment. Therefore, the N_2 adsorption/desorption isotherm analysis (data not shown here) indicates a lower specific surface area (S_{BET}) value of N-RGO (355 m^2 g^{-1}) in comparison with RGO (482 m^2 g^{-1}). Nevertheless, the electrolyte-accessible surface area of N-RGO and RGO is pretty similar, which will be discussed in Section 3.2.

Besides the morphology characterization, XPS analysis was employed to unravel the composition of elements for RGO and N-RGO (see Fig. 2 and Table 1). Similar contents of carbon and oxygen elements were found. The content of oxygen decreases significantly from 32.7 at% for GO to ca. 13–16 at% for both RGO and N-RGO due to the removal of surface oxygen-containing functional groups via the microwave-assisted hydrothermal treatment [17,19,23]. From a comparison of the XPS data of RGO and N-RGO, about 3.0 at% oxygen on RGO has been replaced by nitrogen to form the N-RGO through the simultaneous reduction and nitrogen doping of GO under the microwave-assisted hydrothermal environment and therefore the nitrogen content on N-RGO is 3.0 at%. Since the microwave-assisted hydrothermal treatment is a relatively low-temperature process (190 °C), the reaction between the surface functional groups on GO nanosheets and urea mainly results in the incorporation of nitrogen atoms to the peripheral graphitic structure of graphene, leading to the formation of

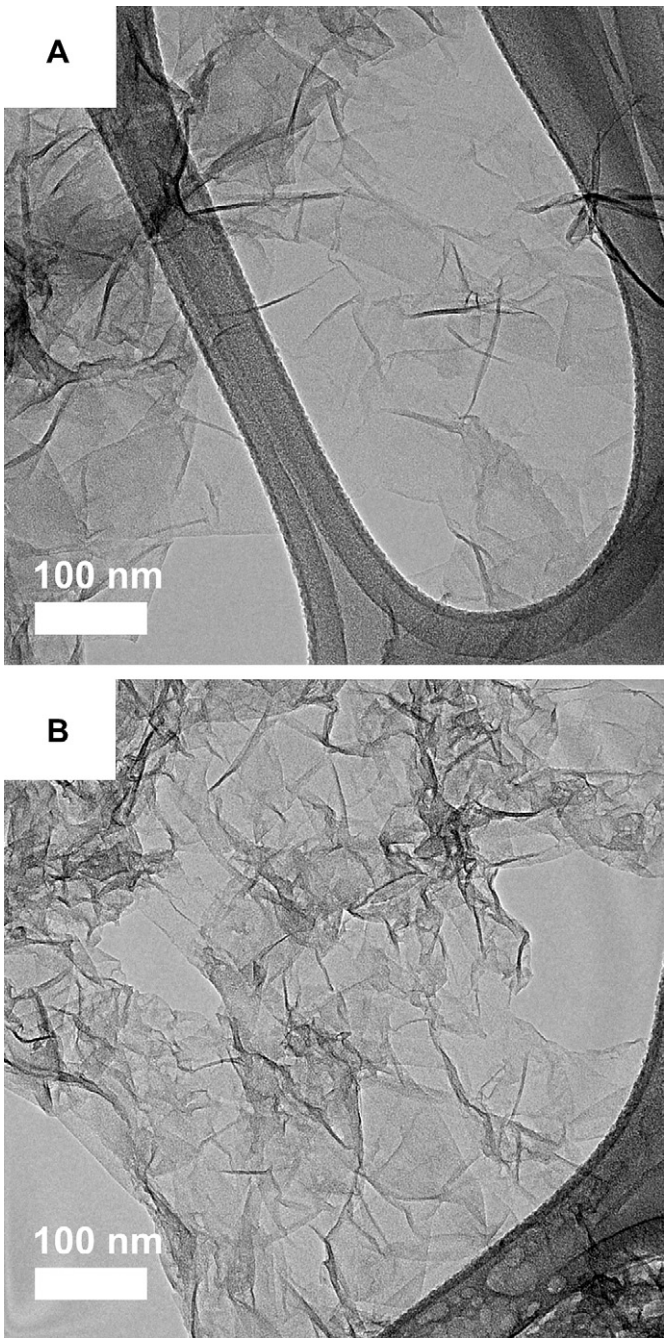

Fig. 1. TEM images of (A) RGO and (B) N-RGO.

pyridinic-N (N-6) and pyrrolic-N/pyridone-N (N-5) structures (Fig. 2). Because the quaternary-N (N-Q) is more likely to appear at the temperature above 750 °C via a thermal process in vacuum [24–26], its content is much lower. Different types of nitrogen-containing functional groups are deconvoluted from the XPS spectrum of N-RGO in Fig. 2 (N-6: 398.5 eV, N-5: 400 eV, N-Q: 401.2 eV, and N-X: 403 eV [1,4,10]) and their contents are summarized in Table 1. In addition, the chemical form of oxygen-containing functional groups is also deconvoluted from the XPS core-level spectra of O 1s (data not shown here) and summarized in Table 1. Three types of oxygen-containing functional groups are found in RGO and N-RGO: quinone-type group (C=O, 531 eV), phenol group and ester group (C–OH and O–C–O, 532 eV), and

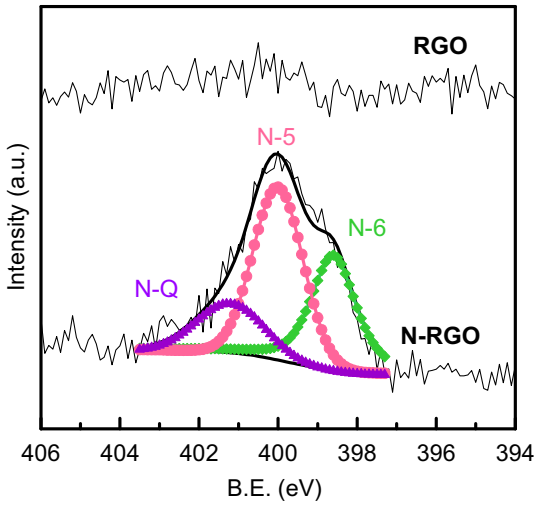

Fig. 2. N 1s core-level XPS spectra of RGO and N-RGO. The black line is the raw-spectrum; the green ◆, pink ●, and purple ▲ lines correspond to pyridinic nitrogen (N-6), pyrrolic nitrogen/pyridone nitrogen (N-5), and quaternary nitrogen (N-Q), respectively (For interpretation of the references to colour in this figure legend, the reader is referred to the web version of this article.).

carboxylic group and chemisorbed oxygen (COOH, 535 eV) [1,10]. According to previous study [1,27–31], quinone-type groups provide pseudo-capacitance through Faradaic redox reactions (see equation (6)) whereas the other two types of functional groups are not electrochemically active. The redox reaction of quinone is pH-dependant. More pronounced pseudocapacitance can be obtained from the redox reaction when pH values of the electrolyte are lower than 3.0 (i.e., sufficient amount of proton in the solution) [28].

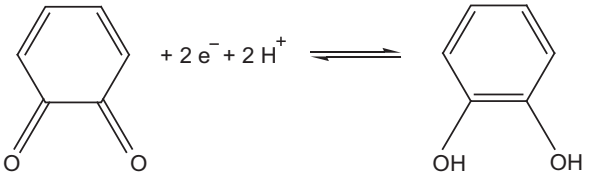

(6)

Since the amount of electrochemically active quinone-type group for RGO and N-RGO is almost the same, the pseudocapacitance contribution from the overall oxygen-containing functional groups for RGO and N-RGO is expected to be the same. Therefore, despite slight difference observed in the oxygen content between RGO and N-RGO, only the variation in the nitrogen content should be responsible for the difference in the capacitive performances.

In addition to the morphology and the content of surface functional groups, the graphitic crystallinity of RGO and N-RGO was examined by the Raman spectra shown in Fig. 3. The spectrum of GO is also added for a comparison purpose. Both D band and G band around 1335 cm^{-1} and 1590 cm^{-1}, respectively, are visible on GO, RGO, and N-RGO [32]. The intensity ratio of D band to G band (I_D/I_G) is 1.15 for both GO and RGO whereas the ratio is slightly higher for N-RGO ($I_D/I_G = 1.25$). The slightly higher intensity of D band should

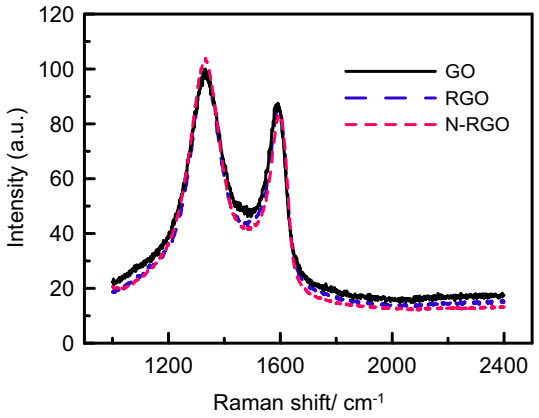

Fig. 3. Raman spectra of GO, RGO, and N-RGO obtained at 633 nm excitation.

result from the additional defects introduced by the N-doping structures. The quite similar intensity ratio for the three materials is ascribed to the reduction mechanism of GO via the microwave-assisted hydrothermal method which simply removes the surface oxygen-containing functional groups without restoring the defects existing on the graphene sheets. Therefore, no significant difference is found in the Raman spectra between GO, RGO, and N-RGO, which is in agreement with our previous work [17]. The similar graphitic crystallinity of RGO and N-RGO indicates that the two materials should exhibit similar electronic conductivity.

To sum up, the material characterization confirms that RGO and N-RGO synthesized by means of the microwave-assisted hydrothermal method display very similar morphology, electrolyte-accessible surface area, and electronic conductivity, except the presence of nitrogen-containing functional groups in N-RGO. Accordingly, RGO and N-RGO are desired materials for discerning the actual contribution of N doping on the capacitive performances of carbon materials for EDLCs.

3.2. Electrochemical characteristics of RGO and N-RGO in H_2SO_4

Typical cyclic voltammograms (CVs) of RGO and N-RGO measured at 25 mV s^{-1} in 1 M H_2SO_4 are shown in Fig. 4A. On the positive sweep of curve 1 for RGO, the voltammetric current density gradually increases with the positive shift in the electrode potential and reaches a maximum at ca. 0.6 V. Then, a constant-current response is found at potentials positive than 0.8 V, attributable to the double-layer response [33]. In addition, the broad but symmetric redox peaks on the positive and negative sweeps of curve 1 have been attributed to the combined contribution of the double-layer and Faradaic redox capacitances [28,33]. Due to the symmetric *i–E* responses of curve 1, RGO is an ideal electrode material of supercapacitors employing aqueous acidic electrolytes. From a comparison of curve 1 and 2, two features have to be mentioned. First, the voltammetric current densities of RGO and N-RGO at potentials positive than 0.6 V are quite close, indicating the similar double layer responses for RGO and N-RGO although the specific surface area of the former material (482 m^2 g^{-1}) is higher than that of the latter (355 m^2 g^{-1}). Accordingly, the double-layer

Table 1
The atomic ratio and deconvolution results (in at%) of the N 1s and O 1s XPS core-level spectra for RGO and N-RGO.

	C (%)	N (%)	O (%)	N-6 (%)	N-5 (%)	N-Q (%)	C=O (%)	C–OH,O–C–O (%)	COOH (%)
RGO	84.0	–	16.0	–	–	–	3.8	7.1	5.1
N-RGO	84.4	3.0	12.6	1.0	1.4	0.6	4.1	5.9	2.6

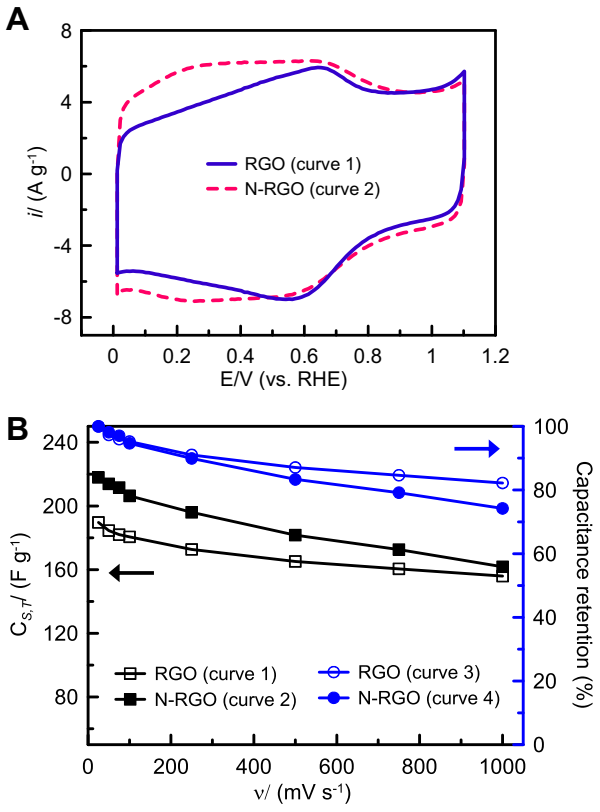

Fig. 4. (A) Cyclic voltammograms measured in 1 M H_2SO_4 at 25 mV s^{-1} and (B) the total specific capacitance ($C_{S,T}$) and capacitance retention (based on the value obtained at 25 mV s^{-1}) against the scan rate of CV for RGO and N-RGO.

capacitance per unit surface area (μF cm^{-2}) of N-RGO should be higher than that of RGO. This phenomenon is attributed to (1) the smaller nanosheets of N-RGO with more exposure of edges (see TEM images in Fig. 1) since higher edge/basal orientation ratio leads to larger specific double-layer capacitance (μF cm^{-2}) [34,35] and (2) the presence of nitrogen changes the electronic state of the graphene sheets to facilitate the adsorption of ions in the electrolyte to improve the specific capacitance [36]. Second, significant higher voltammetric current densities on curve 2 (N-RGO) are clearly visible at electrode potentials negative to 0.6 V, leading to the larger total specific capacitance for N-RGO ($C_{S,T}$ = 218 F g^{-1}) compared to that of RGO ($C_{S,T}$ = 189.6 F g^{-1}). Clearly, the nitrogen-doped functional groups on N-RGO show a significant contribution in Faradaic redox capacitance. This phenomenon is well consistent with the XPS results and the findings in the literature, that pyridinic-N and pyrrolic-N/pyridone-N can provide pseudocapacitance through the redox reactions involving protons [3,6,7,9,11,37]. From the literature, the possible redox reactions are simply expressed as follows:

For pyridinic-N [7,11]:

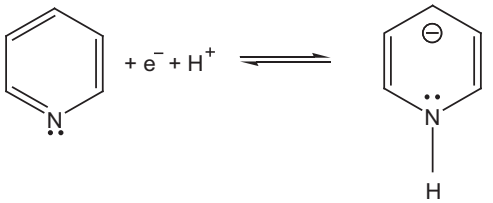

(7)

For pyrrolic-N [3,11]:

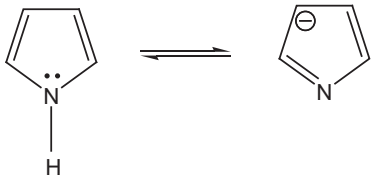

(8)

For pyridone-N [37]:

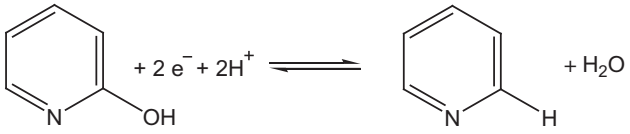

(9)

All the above redox reactions involve proton (or H_2O/OH^-) exchange during the redox transitions. Based on the redox properties of quinone-type groups, the pH range suitable for the above redox reactions should be different from one another, leading to the different pseudocapacitance values when N-RGO was measured in the acidic and basic media.

The dependences of $C_{S,T}$ and capacitance retention on the scan rate of CV are shown in Fig. 4B. Clearly, $C_{S,T}$ of both RGO and N-RGO monotonously decrease with increasing the scan rate of CV. The more obvious decay in $C_{S,T}$ on curves 1 and 2 in the low-scan rate region (≤100 mV s^{-1}) is attributable to the relatively slower electrochemical kinetics of the redox couples coming from O-/N-containing functional groups in comparison with the double-layer charge/discharge responses. From a comparison of curves 3 and 4, capacitance retention for RGO is somewhat better than that of N-RGO since only about 18% loss in $C_{S,T}$ is found for RGO when the scan rate is increased from 25 to 1000 mV s^{-1} while 28% loss is found for N-RGO under the same testing condition. This phenomenon is reasonable because N-RGO shows higher pseudocapacitance than that of RGO from the CV curves shown in Fig. 4A.

Due to the similar double-layer current density between RGO and N-RGO as well as their very similar material characteristics, the capacitive performance differences are attributable to the presence of nitrogen-containing functional groups. Therefore, it is possible to compare the respective contribution of pseudocapacitance from RGO and N-RGO. Because of the relatively slower electrochemical kinetics of the redox couples coming from both O- and N-containing functional groups compared to the double-layer process, $C_{S,T}$ is proposed to be partitioned into pseudocapacitance and double-layer capacitance through utilizing the same procedure in estimating the outer electroactive sites of metal oxides [38–40]. In the partition procedure, the total voltammetric charge, q_T, is given from the extrapolation of voltammetric charge, q, to $v = 0$ from the plot of $1/q$ vs. $v^{1/2}$ (see Fig. 5B). The double-layer charge, q_{dl} (very similar to the outer voltammetric charge, q_o, of metal oxides), can be estimated from the extrapolation of q to $v = \infty$ from the plot of q vs. $v^{-1/2}$ (see Fig. 5A). Accordingly, the pseudocapacitance charge, q_p, can be obtained from the difference between q_T and q_{dl}. In addition, $C_{S,T,M}$, $C_{S,dl}$, and $C_{S,p}$ corresponding to the maximum total specific capacitance, double-layer capacitance, and pseudocapacitance can be obtained by dividing the charge with the potential window of CV (i.e., 1.1 V in this work), which are summarized in Table 2. Owing to the presence of abundant oxygen-containing functional groups, 11.3% of $C_{S,T,M}$ comes from pseudocapacitance for RGO is shown in Table 2, which is provided from the redox reaction of the quinone groups [27–30], as mentioned in Section

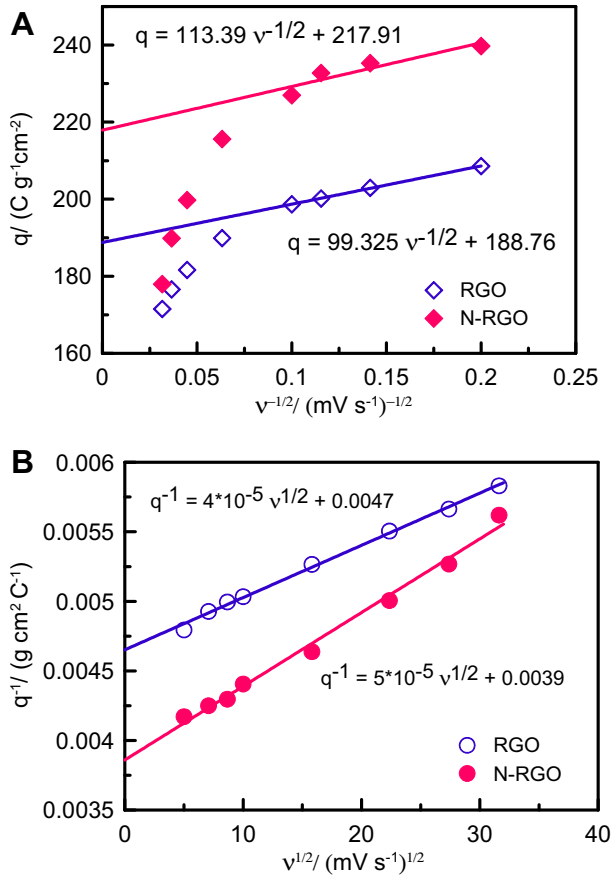

Fig. 5. (A) Dependence of q on $v^{-1/2}$ and (B) dependence of $1/q$ on $v^{1/2}$ for RGO and N-RGO in 1 M H_2SO_4.

3.1. The redox peaks can be clearly observed in Fig. 4A. However, for N-doped GS, ca. 4% more pseudocapacitance is obtained due to the contribution of nitrogen-containing functional groups. Since the possible redox reactions for N-6 and N-5 shown as equations (7)–(9) generally involve exchange of protons (or H_2O/OH^-), some of these redox reactions may be favorable in the acidic electrolytes. Hence, ca. 4% more pseudocapacitance donated from N-6 and N-5 other than the contribution of quinone types is obtained. Larger amounts of N-6 and N-5 revealed in the XPS analysis further confirmed the additional pseudocapacitance resulting from the contribution of these functional groups. Since the functional groups on graphene cannot undergo redox reactions thoroughly during the fast charge/discharge process and the fact that N-RGO contains more functional groups (i.e., N-6 and N-5), more significant capacitance drop can be observed at higher scan rates compared to that of RGO (as indicated in Fig. 4B previously). However, the presence of additional pseudocapacitance from N-6 and N-5 still contributes to the higher total specific capacitance for N-RGO at all scan rates.

Table 2
Summary of maximum total specific capacitance ($C_{S,T,M}$), double-layer capacitance (C_{dl}), and pseudocapacitance (C_p) for RGO and N-RGO from the plots of q vs. $v^{-1/2}$ and $1/q$ vs. $v^{1/2}$.

Electrolyte	Sample	$C_{S,T,M}$ (F g^{-1})	C_{dl} (F g^{-1})	C_p (F g^{-1})	$C_p/C_{S,T,M}$ (%)
1 M H_2SO_4	RGO	193.4	171.6	21.8	11.3
	N-RGO	233.1	198.1	35	15
1 M KOH	RGO	206.6	184.7	21.9	10.6
	N-RGO	185.5	161.9	23.6	12.7

The Ragone plots of N-RGO and RGO are shown in Fig. 6 meanwhile the results of activated carbon (AC) and carbon nanotubes (CNTs) are also attached for comparison. The good electrical conductivity of these carbon materials renders themselves high specific power (SP) near or more than 10 kW kg^{-1}. However, the specific energy (SE) varies a lot within these materials. Low SE is found for AC (1.8 W h kg^{-1}) and CNT (0.4 W h kg^{-1}) due to their small specific capacitance. But SE for N-RGO and RGO is 8.4 W h kg^{-1} and 6 W h kg^{-1}, respectively. Higher SE is obtained for N-RGO owing to the incorporation of nitrogen-containing functional groups, i.e., N-6 and N-5, which provides more pseudocapacitance to increase the SE of the system. The result indicates that N-doping on the carbon material with higher total specific capacitance shows great potential as the electrode materials of EDLCs when operating in the acidic electrolytes.

In the acidic electrolyte, the presence of nitrogen-containing functional groups not only provides more pseudocapacitance, but also enhances the double layer capacitance. As shown in Table 2, the double layer capacitance of N-RGO is higher than that of RGO, which may be ascribed to the change in surface charge due to the presence of more basic nitrogen-containing functional groups. For RGO, only oxygen-containing functional groups exist on the surface of graphene. The amount of acidic groups, such as carboxylic groups or lactones, are usually more than that of basic and neutral groups (such as phenols, ethers, and carbonyls) [30], which constitutes the acidic surface nature of RGO [1,10]. On the other hand, introducing nitrogen-containing functional groups makes the surface more basic, especially for the carbons with high contents of N-6 and N-5 groups [1,10]. This enhanced basicity of N-RGO increases the electronic charge density of graphene and favors the proton adsorption in the acidic electrolyte [27,29,41,42]. Consequently, the incorporation of nitrogen-containing functional groups shows beneficial effects on the capacitive performance in the acidic electrolyte; they not only provide pseudocapacitance through redox reactions but also change the surface charge to enhance double-layer capacitance. Therefore, N-doping on carbon materials is promising for an EDLC when operating in the acidic electrolyte.

3.3. Electrochemical characteristics of RGO and N-RGO in KOH

Fig. 7A shows the CVs of N-RGO and RGO in 1 M KOH. Contrary to the CVs obtained in 1 M H_2SO_4, the current response of N-RGO is

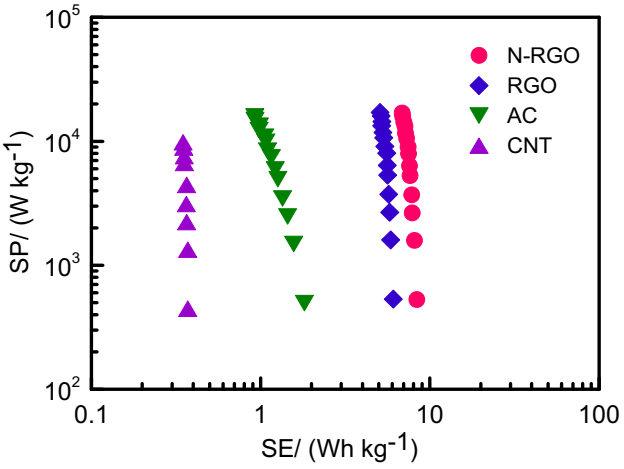

Fig. 6. Ragone plots of N-RGO, RGO, activated carbon (AC), and carbon nanotubes (CNTs) obtained in 1 M H_2SO_4.

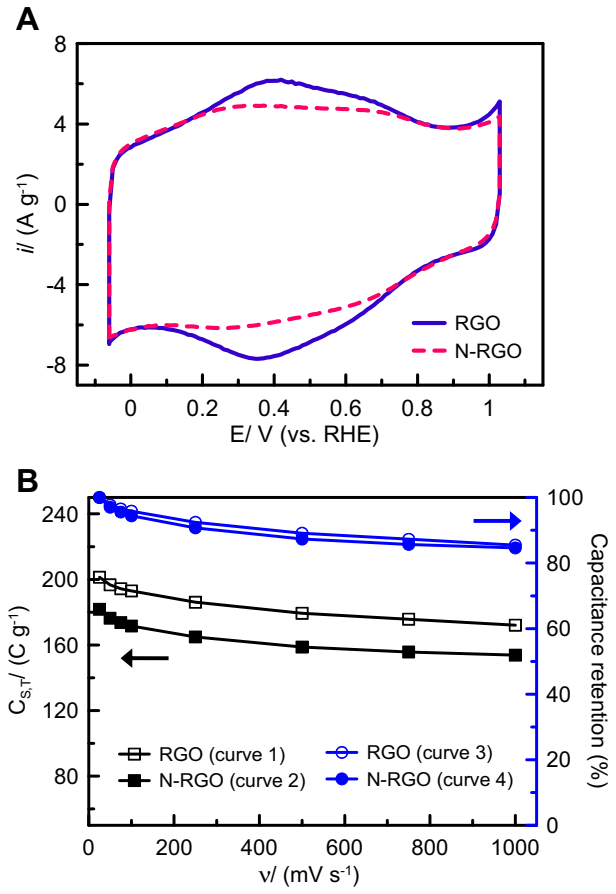

Fig. 7. (A) Cyclic voltammograms measured in 1 M KOH at 25 mV s^{-1} and (B) the total specific capacitance ($C_{S,T}$) and capacitance retention (based on the value obtained at 25 mV s^{-1}) against the scan rate of CV for RGO and N-RGO.

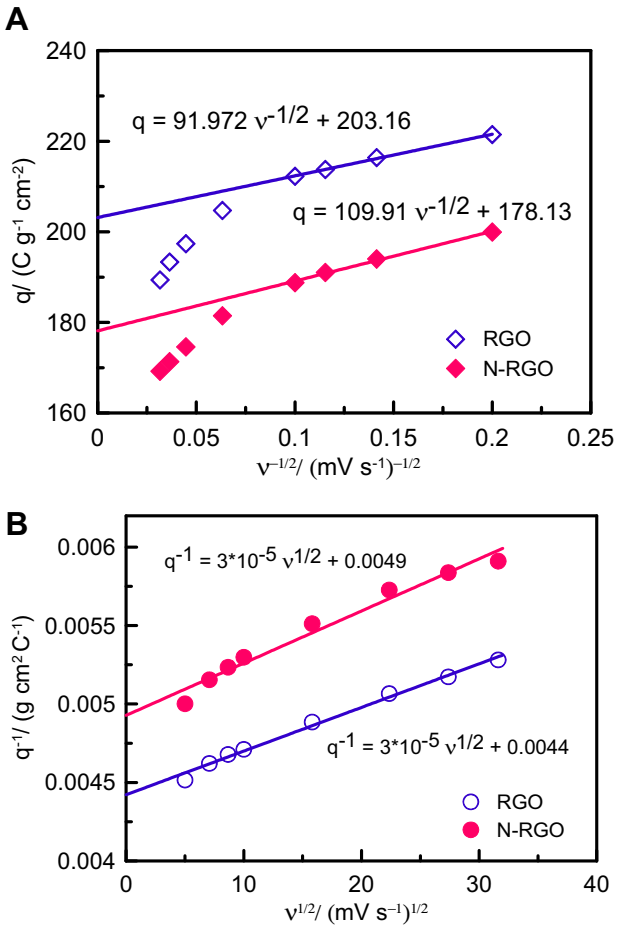

Fig. 8. (A) Dependence of q on $v^{-1/2}$ and (B) dependence of $1/q$ on $v^{1/2}$ for RGO and N-RGO in 1 M KOH.

smaller than that of RGO in 1 M KOH. The specific capacitance of N-RGO and RGO is 181.8 and 201.3 F g^{-1}, respectively. Again, the maximum total specific capacitance ($C_{S,T,M}$ extrapolated at the scan rate = 0 mV s^{-1}) can be partitioned into pseudocapacitance and double-layer capacitance through the same procedure employed in Fig. 5 (see Fig. 8A and B) and data are summarized in Table 2. The percentage of pseudocapacitance from N-RGO is only slightly higher than that of RGO, which leads to similar capacitance retention at high scan rates (84.6% for N-RGO and 85.5% for RGO at 1000 mV s^{-1}), as shown in Fig. 7B. Note that the pseudocapacitance contribution from both N-RGO and RGO is smaller than that obtained in the acidic electrolyte. Previous study indicates that only "basic" oxygen-containing functional groups, i.e., quinone groups, contribute to the pseudocapacitance and such contribution is more pronounced in acid than in alkaline [28,43]. Since N-RGO contains more basic functional groups (i.e., nitrogen-containing functional groups) besides quinone groups, the contribution of pseudocapacitance should be more significant in the acidic electrolyte in comparison with the alkaline electrolyte. Indeed, the estimated pseudocapacitance for N-RGO in 1 M H_2SO_4 is 35 F g^{-1} whereas it decreases to 23.6 F g^{-1} in 1 M KOH. The lack of proton in the electrolyte suppresses the redox reactions of N-6 and N-5, which in turn leads to the loss of pseudocapacitance. A similar phenomenon is expected for RGO since its pseudocapacitance is contributed mostly by the redox reaction of quinone/hydroquinone [28,43]. However, nearly the same estimated value of pseudocapacitance in both acidic and alkaline electrolytes is obtained for RGO. Although the redox reaction for quinone would be suppressed in 1 M KOH, certain functional groups such as protonated pyrone (at least three pyrone-like groups) which shows no electrochemical activity in acids might exhibit activity in the alkaline electrolyte and provide additional pseudocapacitance [28,44]. Consequently, the pseudocapacitance from pyrone-like groups compensates the capacitance loss from quinone groups, leading to the pseudocapacitance close to that obtained in 1 M H_2SO_4.

In addition to the decrease in pseudocapacitance, N-RGO also demonstrates a smaller double-layer capacitance value in 1 M KOH, which accounts for the slightly larger percentage of pseudocapacitance for N-RGO than that of RGO. The exact reasons responsible for the different variations in the double-layer capacitance obtained in alkaline and acidic electrolytes for RGO and N-RGO are not clear. It is probably due to the size of hydrated ions (the order of hydrated ions with respect to increasing the hydrated ionic size is: $OH^- < K^+ \sim H_3O^+$ (3.62–4.2 Å) $< SO_4^{2-}$ (5.33 Å) [16]) and the electrostatic interactions between hydrated ions and carbons as well as the specific adsorption of hydrated/partially hydrated ions. The double-layer capacitance of N-RGO obtained in the alkaline electrolyte is smaller than that measured in the acidic electrolyte, implying that the specific adsorption of hydrated ions has been suppressed, probably due to the basic surface nature of N-RGO (i.e., an increase in the electronic charge density) owing to the presence of nitrogen-containing functional groups. In short, the results demonstrate that the influences of nitrogen-containing functional groups on the capacitive performance of carbons are strongly dependent on pH of the electrolyte and that both

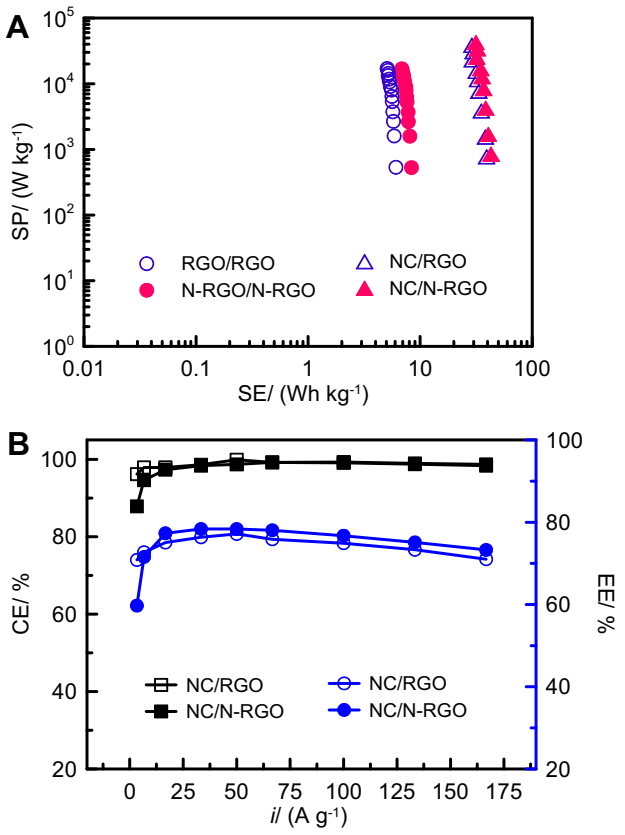

Fig. 9. (A) Ragone plots and (B) Coulombic efficiency (CE) and energy efficiency (EE) of an asymmetric supercapacitor consisting of a nickel–cobalt hydroxide positive electrode and an N-RGO (or RGO) negative electrode in 1 M KOH. Symmetric supercapacitor consisting of RGO/RGO or N-RGO/N-RGO in 1 M H_2SO_4 is added in (A) for comparison.

the pseudocapacitance and double-layer capacitance of N-doped carbons diminish in the alkaline electrolyte.

Despite the slightly inferior capacitive performance of N-RGO than that of RGO, N-RGO still exhibits the potential for the electrode materials of ECs in the asymmetric design in the alkaline electrolyte. Both N-RGO and RGO are employed as the negative electrode materials in combination with Ni–Co hydroxide as the positive electrode to construct the asymmetric two-electrode systems (denoted as NC/N-RGO and NC/RGO, respectively). The Ragone plots of the above two asymmetric systems are shown in Fig. 9A. Interestingly, both the utilization of N-RGO and RGO as the negative electrode demonstrates similar SE and SP. Furthermore, the energy efficiency for the NC/N-RGO system is slightly higher than that of the NC/RGO design (see Fig. 9B), indicating that the employment of N-RGO in the alkaline electrolyte still shows promising effects.

4. Conclusions

N-doped RGO and RGO with similar material characteristics yet different in the nitrogen content have been successfully synthesized via the microwave-assisted hydrothermal method, which are the typical materials for evaluating the actual contribution of nitrogen-containing functional groups in acidic and alkaline electrolytes. The capacitance contribution from the nitrogen-containing functional groups is more significant in the acidic electrolyte than in the alkaline medium due to the facts that protons favor the redox reactions of pyridinic-N and pyrrolic-N/pyridone-N to provide additional pseudocapacitance and the higher electronic charge density of N-RGO facilitates ion adsorption to enhance the double-layer capacitance. Despite the capacitive performance of N-doped GS in alkaline being slightly inferior to that in acid, this material employed as the negative electrode in an asymmetric EC shows more positive effects in comparison with RGO, indicating the promising potential of N-doping for carbon-based electrode materials in both acidic and alkaline electrolytes.

Acknowledgments

The financial supports of this work, the National Science Council of ROC-Taiwan under contract no. NSC 100-2628-E-007-028-MY2 and the boost program from the Low Carbon Energy Research Center of National Tsing Hua University, are gratefully acknowledged.

References

[1] D. Hulicova-Jurcakova, M. Seredych, G.Q. Lu, T.J. Bandosz, Advanced Functional Materials 19 (2009) 438.
[2] Y.J. Kim, Y. Abe, T. Yanagiura, K.C. Park, M. Shimizu, T. Iwazaki, S. Nakagawa, M. Endo, M.S. Dresselhaus, Carbon 45 (2007) 2116.
[3] E. Frackowiak, G. Lota, J. Machnikowski, C. Vix-Guterl, F. Béguin, Electrochimica Acta 51 (2006) 2209.
[4] T.E. Rufford, D. Hulicova-Jurcakova, Z. Zhu, G.Q. Lu, Electrochemistry Communications 10 (2008) 1594.
[5] H. Wang, Q. Gao, J. Hu, Microporous and Mesoporous Materials 131 (2010) 89.
[6] D. Hulicova-Jurcakova, M. Kodama, S. Shiraishi, H. Hatori, Z.H. Zhu, G.Q. Lu, Advanced Functional Materials 19 (2009) 1800.
[7] G. Lota, K. Lota, E. Frackowiak, Electrochemistry Communications 9 (2007) 1828.
[8] K. Jurewicz, K. Babeł, R. Pietrzak, S. Delpeux, H. Wachowska, Carbon 44 (2006) 2368.
[9] H.M. Jeong, J.W. Lee, W.H. Shin, Y.J. Choi, H.J. Shin, J.K. Kang, J.W. Choi, Nano Letters 11 (2011) 2472.
[10] M. Seredych, D. Hulicova-Jurcakova, G.Q. Lu, T.J. Bandosz, Carbon 46 (2008) 1475.
[11] E. Frackowiak, Physical Chemistry Chemical Physics 9 (2007) 1774.
[12] N.D. Kim, W. Kim, J.B. Joo, S. Oh, P. Kim, Y. Kim, J. Yi, Journal of Power Sources 180 (2008) 671.
[13] K. Jurewicz, K. Babeł, A. Źiółkowski, H. Wachowska, Electrochimica Acta 48 (2003) 1491.
[14] D. Hulicova-Jurcakova, J. Yamashita, Y. Soneda, H. Hatori, M. Kodama, Chemistry of Materials 17 (2005) 1241.
[15] L. Zhao, L.-Z. Fan, M.-Q. Zhou, H. Guan, S. Qiao, M. Antonietti, M.-M. Titirici, Advanced Materials 22 (2010) 5202.
[16] D. Hulicova-Jurcakova, M. Kodama, H. Hatori, Chemistry of Materials 18 (2006) 2318.
[17] J.-L. Chang, K.-H. Chang, C.-C. Hu, W.-L. Cheng, J.-M. Zen, Electrochemistry Communications 12 (2010) 596.
[18] S. Park, J. An, R.D. Piner, I. Jung, D. Yang, A. Velamakanni, S.T. Nguyen, R.S. Ruoff, Chemistry of Materials 20 (2008) 6592.
[19] Y. Zhou, Q. Bao, L.A.L. Tang, Y. Zhong, K.P. Loh, Chemistry of Materials 21 (2009) 2950.
[20] C.N.R. Rao, A.K. Sood, K.S. Subrahmanyam, A. Govindaraj, Angewandte Chemie International Edition 48 (2009) 7752.
[21] S. Stankovich, D.A. Dikin, G.H.B. Dommett, K.M. Kohlhaas, E.J. Zimney, E.A. Stach, R.D. Piner, S.T. Nguyen, R.S. Ruoff, Nature 442 (2006) 282.
[22] K.-H. Chang, Y.-F. Lee, C.-C. Hu, C.-I. Chang, C.-L. Liu, Y.-L. Yang, Chemical Communications 46 (2010) 7957.
[23] D. Long, W. Li, L. Ling, J. Miyawaki, I. Mochida, S.-H. Yoon, Langmuir 26 (2010) 16096.
[24] R. Kothandaraman, V. Nallathambi, K. Artyushkova, S.C. Barton, Applied Catalysis B: Environmental 92 (2009) 209.
[25] H. Chen, Y. Yang, Z. Hu, K. Huo, Y. Ma, Y. Chen, X. Wang, Y. Lu, Journal of Physical Chemistry B 110 (2006) 16422.
[26] X. Li, H. Wang, J.T. Robinson, H. Sanchez, G. Diankov, H. Dai, Journal of the American Chemical Society 131 (2009) 15939.
[27] Y.-R. Nian, H. Teng, Journal of the Electrochemical Society 149 (2002) A1008.
[28] H.A. Andreas, B.E. Conway, Electrochimica Acta 51 (2006) 6510.
[29] D.-W. Wang, F. Li, M. Liu, H.-M. Cheng, New Carbon Materials 22 (2007) 307.
[30] M.J. Bleda-Martínez, J.A. Maciá-Agulló, D. Lozano-Castelló, E. Morallón, D. Cazorla-Amorós, A. Linares-Solano, Carbon 43 (2005) 2677.
[31] K. Okajima, K. Ohta, M. Sudoh, Electrochimica Acta 50 (2005) 2227.
[32] S. Reich, C. Thomsen, Philosophical Transactions of The Royal Society A: Mathematical, Physical and Engineering Sciences 362 (2004) 2271.
[33] R. Kötz, M. Carlen, Electrochimica Acta 45 (2000) 2483.
[34] A.G. Pandolfo, A.F. Hollenkamp, Journal of Power Sources 157 (2006) 11.
[35] D. Qu, Journal of Power Sources 109 (2002) 403.
[36] Z.H. Zhu, H. Hatori, S.B. Wang, G.Q. Lu, Journal of Physical Chemistry B 109 (2005) 16744.

[37] D.-W. Wang, F. Li, L.-C. Yin, X. Lu, Z.-G. Chen, I.R. Gentle, G.Q.M. Lu, H.-M. Cheng, Chemistry—A European Journal 18 (2012) 5345.
[38] S. Ardizzone, G. Fregonara, S. Trasatti, Electrochimica Acta 35 (1990) 263.
[39] D. Baronetto, N. Krstajic, S. Trasatti, Electrochimica Acta 39 (1994) 2359.
[40] K.-H. Chang, C.-C. Hu, C.-Y. Chou, Chemistry of Materials 19 (2007) 2112.
[41] H. Gerischer, Journal of Physical Chemistry 89 (1985) 4249.
[42] R.L. McCreery, K.K. Cline, C.A. McDermott, M.T. McDermott, Colloids and Surfaces A: Physicochemical and Engineering Aspects 93 (1994) 211.
[43] V. Barranco, M.A. Lillo-Rodenas, A. Linares-Solano, A. Oya, F. Pico, J. Ibanez, F. Agullo-Rueda, J.M. Amarilla, J.M. Rojo, Journal of Physical Chemistry C 114 (2010) 10302.
[44] E. Fuente, J.A. Menéndez, D. Suárez, M.A. Montes-Morán, Langmuir 19 (2003) 3505.